A Passive Mechanism for Relocating Payloads with a Quadrotor

Joseph DeGol, David Hanley, Navid Aghasadeghi, and Tim Bretl

***Abstract*— We present a passive mechanism for quadrotor vehicles and other hover-capable aerial robots based on the cam-follower. This mechanism has two mating parts, one attached to the quadrotor and the other attached to a payload. These two parts are joined by a toggle switch—push to connect, push to disconnect—that is easy to activate with the quadrotor by varying thrust. We discuss the design parameters and provide an inertial model for our mechanism. With hardware experiments, we demonstrate the use of this passive mechanism to autonomously place a wireless camera in several different locations on the underside of a steel beam. Our mechanism is open source and can be easily fabricated with a 3D printer.**

I. INTRODUCTION

This paper presents a passive mechanism that enables a quadrotor and other hover-capable unmanned aerial vehicles to relocate payloads (Figure 1). It consists of two mating parts: one attached to the quadrotor and the other attached to the payload. These two pieces function as a toggle switch—they connect when pushed together, and disconnect when pushed together again. Magnets enable the mechanism to be placed on and removed from flat metal surfaces. We present a systematic approach for choosing mass and dimension parameters. Through 320 docking trials, we show a mean docking time of 13.8 seconds and a 90% probability of docking within 25 seconds. Finally, we demonstrate our mechanism being used to move a camera between three locations on a metal beam. Our mechanism is open source and can be fabricated with a 3D printer[1].

Related work by Doyle et. al. [1] provides an avian-inspired design of a passive claw for perching on surfaces under the vehicle where tendons are actuated by the mass of the UAV. Active claws are an alternative approach. Work by Mellinger et. al. [2] presents the design of an ingressive claw and demonstrates its use for aerial grasping and perching. Similar work by Thomas et. al. [3] takes inspiration from raptors for the design and demonstration of avian grasping and perching. Work by Backus et. al. [4] provides results on how pulley ratio, object size, and palm size affect grasping performance for claws on UAVs. Active manipulators have also been designed for UAVs. Work by Danko et. al. [5] considers the design of a nine-joint manipulator hanging below a quadrotor and demonstrates its use for pick and place. Finally, Fumagalli et. al. [6], [7] present the design of a cardan gimbal inspired end-effector for quadrotor inspection of boilers and chimneys. Inspired by these works, we design a passive mechanism, which can be activated by the vertical motion of the quadrotor, and used to relocate objects.

J. DeGol, D. Hanley, N. Aghasadeghi, and T. Bretl are with the University of Illinois, Urbana, IL 61801, USA {degol2, hanley6, aghasad1, tbretl}@illinois.edu, bretl.csl.illinois.edu

[1]http://bretl.csl.illinois.edu/projects/aerialmonitoring

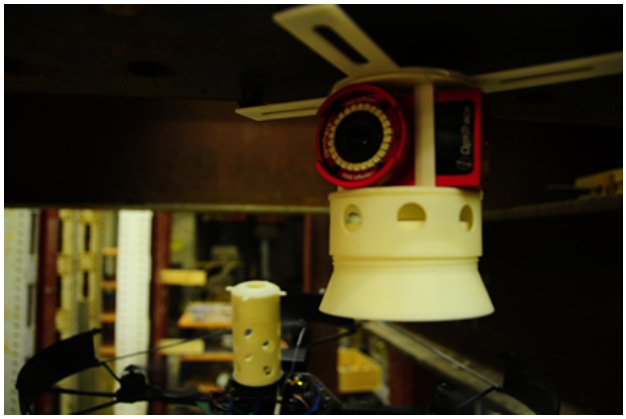

Fig. 1: The passive mechanism in this paper consists of two mating parts that function like a toggle switch to allow a quadrotor to relocate cameras and other small payloads.

Construction site monitoring can benefit from the ability to relocate cameras using a quadrotor. Construction site monitoring is important for worker safety, blueprint and timeline compliance, and resource management. Due to the evolving nature of a construction site, it is difficult to fix cameras to the structure for daily monitoring tasks. The current solution involves foremen walking the grounds and manually taking photographs [8]. One alternative is to autonomously deploy and relocate a network of cameras on steel beams around the construction site. In principle, our mechanism allows a quadrotor to perform this task.

Section II details the design of our mechanism. Section III describes our algorithm for relocating objects. In Section IV, we present results from 320 docking trials and demonstrate autonomous relocation of a wireless camera on a steel beam. We provide conclusions and future work in Section V.

II. PASSIVE MECHANISM

In this section, we describe the mechanism's components (Section II-A), toggle switch functionality (Section II-B), mass and dimension parameters (Section II-B), and flight dynamics (Section II-D).

A. Components

The mechanism consists of male and female mating parts. We refer to the male part as 1) the *insertion component*. We split the female part into two components based on functionality: 2) the *housing component* and 3) the *holder*

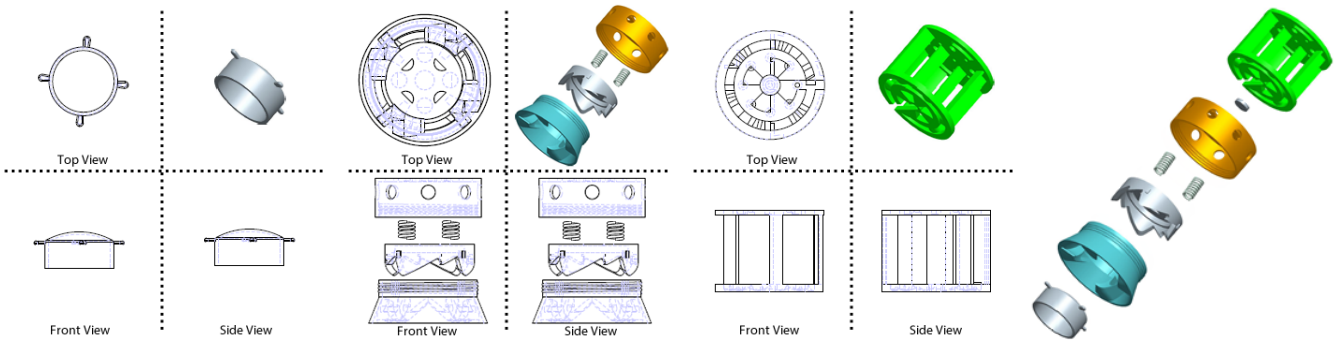

(a) Insertion Component (b) Housing Component (c) Holder Component (d) Exploded View

Fig. 2: Schematics of each mechanism component and an exploded view of the components.

component. Our design is based on the cam-follower that is often found in retractable ballpoint pens [9], [10].

1) The insertion component (Figure 2a) is a cylinder with four teeth that interface with the housing component. This piece is analogous to the follower of the cam-follower mechanism and is fixed to the quadrotor.
2) The housing component (Figure 2b) consists of a base, cap, and inner disk and is analogous to the cam of the cam-follower mechanism. Inside the base, sloped ridges induce rotation when in contact with the teeth of the insertion component and hold the insertion component in place when docking is successful. The cap is screwed on to the base and several springs are attached between the cap and the inner disk. The inner disk also has a set of sloped ridges and presses against the inner ridges of the base. Together, the inner disk and springs serve the same function as the spring and pushbutton of a retractable ballpoint pen.
3) The holder component (Figure 2c) is shaped to hold various payloads as needed. The holder component is attached to the housing component using a bearing. The holder component interfaces with the docking surface (e.g., a steel beam) by attaching to it via magnets. While attached, the holder component is fixed to the surface; however, the housing component is free to rotate about the bearing that connects them. This rotation allows the housing component to align with the teeth of the insertion component during mating.

Figure 2d provides an exploded view of the entire mechanism, including all three components.

B. Toggle Switch Functionality

The insertion and housing components function as a toggle switch. They become connected (1. *Docking*) when pushed together and disconnected (2. *Undocking*) when pushed together again. This process is shown in Figure 4.

1) Docking begins by pushing the insertion component into the housing component and the four teeth of the insertion component contact the ridges along the inside of the housing component (Figure 4a). The sloped ridges force the insertion teeth to induce a rotation on the housing. The housing piece continues to rotate as the teeth move into contact with the spring-loaded inner disk (Figure 4b). The teeth push against the spring-loaded inner disk, forcing it upward as the sloped ridges of the inner disk induce a rotation that moves the insertion teeth to the apex of the ridges of the inner disk (Figure 4c). Decreasing the insertion force drops the teeth into the docking zone (Figure 4d). Docking is complete. These motions equate to a set of rotations for the housing component and an inward push force by the insertion component—push to connect.
2) Undocking proceeds like docking except the insertion component disconnects from the housing component (Figures 4e-4h). The motions equate to a set of rotations by the housing component and an inward push force by the insertion component—push to disconnect.

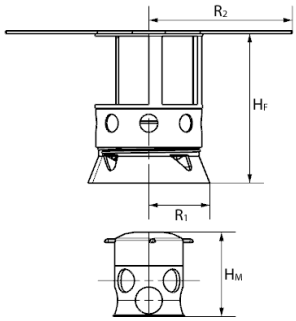

Fig. 3: Mechanism parameters.

C. Choosing Mass and Dimension Parameters

We consider six parameters when designing the mechanism: R_1 (radius of the housing component), R_2 (radius of the top plate of the holder component), H_F (height of the female part), H_M (height of the male part), F_M (magnet force), and F_K (spring force). Figure 3 depicts R_1, R_2, H_F, and H_M. These parameters can be chosen by following a step-by-step approach.

1) We choose H_F based on the height of the intended payload. The height of the housing component remains fixed, but the height of the holder component is adjusted.

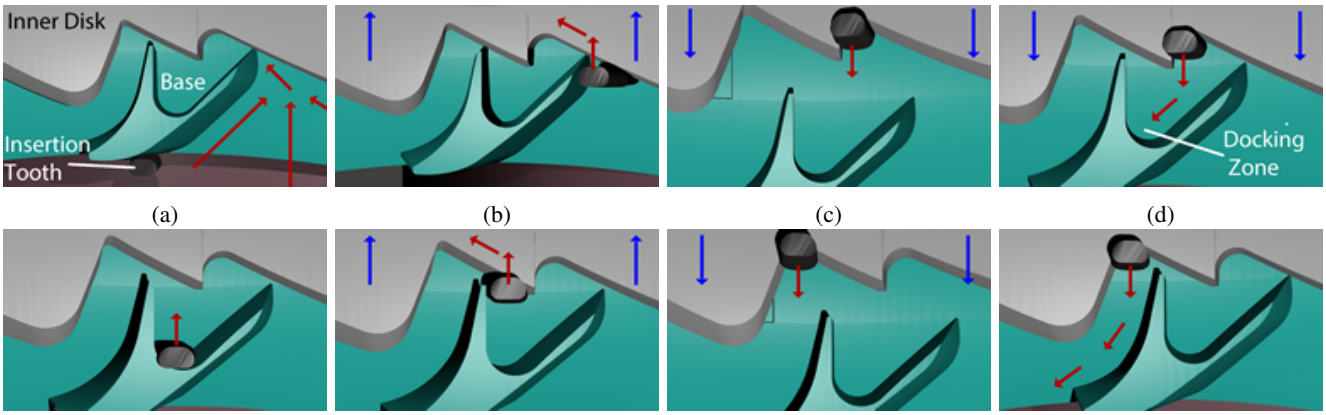

Fig. 4: The docking and undocking procedure for one tooth of the insertion component: The gray and teal sections correspond to the inner disk and base respectively. The black piece is a single tooth of the insertion component. The blue arrows depict the motion of the inner disk and the red arrows depict the motion of the insertion tooth.

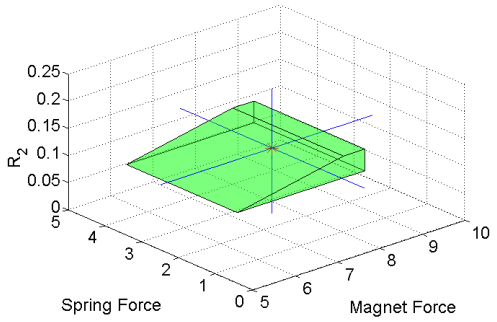

Fig. 5: Feasible region for choosing F_M, F_K, and R_2.

2) While attempting to dock, the quadrotor can slip off the mechanism with an upward thrust. We choose an H_M that is large enough to allow the quadrotor to recover from this failure without hitting the female part of the mechanism. We also want to minimize this height because errors in roll and pitch angle have a larger effect on the positional error of the male part for larger H_M values.
3) We fly the quadrotor at a set position and model the x-y position error as a Gaussian distribution. We then choose R_1 to be equal to the radius of the 3σ covariance ellipse along the major axis.
4) Parameters R_1, R_2, H_F, and H_M define the dimensions of our mechanism. Using CAD models, we calculate the mass of the male (m_M) and female (m_F) parts based on the density of the 3D printing material.
5) We consider force and torque constraints for choosing R_2, K, and F_M. We choose springs that the quadrotor can compress with force generated by thrust. Thus, the first constraint is

$$F_f < F_K < F_Q - F_f - m_Q g \tag{1}$$

where F_f is the friction force from contact between insertion and housing components, F_K is the maximum force the spring can exert, F_Q is our design point maximum force for the quadrotor, m_Q is the mass of the quadrotor, and g is gravity. Note that in practice, $F_f \ll F_Q$ and $F_f \ll F_K$, so we choose to ignore it. The next constraint is that the magnets must be strong enough to hold the female part and payload to a metal surface, but weak enough to be pulled off by the additional weight of a docked male part and quadrotor. This constraint can be written as

$$(m_F+m_P)g < F_M < (m_F+m_P+m_M+m_Q)g \tag{2}$$

where m_P is the mass of the payload. The last constraint is that the magnets must be strong enough to withstand torque caused by the quadrotor. Assuming the magnets are placed symmetrically on the top of the female part, the torque constraint can be written as

$$\begin{aligned} T_Q &< T_M \\ F_{Qxy} &< \frac{R_2}{H_F}(F_M + F_{Qz}) \end{aligned} \tag{3}$$

where F_{Qxy} is the quadrotor force in the horizontal plane and F_{Qz} is the upward quadrotor force. These constraints form a 3-dimensional region in the space of F_M, F_K, and R_2 from which we choose a feasible set of parameters. Figure 5 shows the feasible region for our constraints. We choose the mean point (red star) within the feasible region to provide a buffer for error. Our parameter choices are $R_1 = 0.043\ m$, $R_2 = 0.12\ m$, $H_F = 0.11\ m$, $H_M = 0.1\ m$, $F_M = 12\ N$, and $F_K = 7.63\ N$, with a total mechanism mass of $115\ g$.

D. Flight Mechanics with the Mechanism

The flight mechanics of the quadrotor are altered by the addition of the mechanism. Besides an increase in mass, this alteration manifests itself through the moment of inertia matrix, J, in the equation of rotational dynamics of a general rigid body as expressed in Equation (4).

$$\dot{\omega} = J^{-1}(\tau - \hat{\omega} J \omega) \tag{4}$$

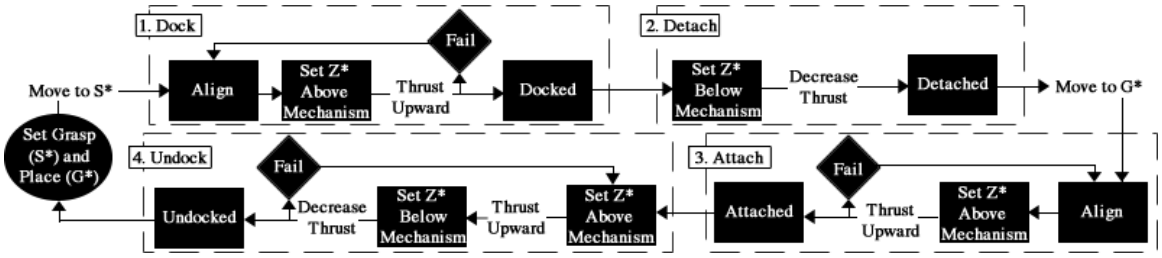

Fig. 6: Flow diagram of our deployment and relocation algorithm.

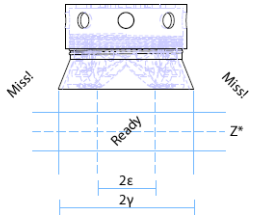

Fig. 7: Aligning with S^* or G^*.

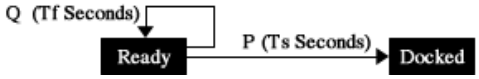

Fig. 8: Markov chain model for docking.

Two cases exist that effect J. These cases are (i) the quadrotor is only carrying the male part and (ii) the quadrotor is carrying both the male and female parts. In case (i), we model the male part as a cylinder and use the parallel axis theorem to find J as shown in equation (5). In case (ii) and with careful choice of payload (compact payloads modeled as point masses), we model the female part as a cylinder and use the same equation for J (Equation (5)).

$$J = J_Q + J_C + \begin{bmatrix} m_{MF}d^2 & 0 & 0 \\ 0 & m_{MF}d^2 & 0 \\ 0 & 0 & 0 \end{bmatrix} \quad (5)$$

Here J_Q is the moment of inertia matrix of the quadrotor, J_C is the moment of inertia matrix of the male part (case i) or the male and female parts (case ii), m_{MF} is the mass of the male part (case i) or the male and female parts (case ii), and d is the distance between the center of mass of the quadrotor and mechanism.

A different J is required for payloads that can not be modeled as point masses and we leave this for future work.

III. Deployment and Relocation Algorithm

In this section, we detail a control algorithm for relocating objects with our mechanism based on approaches outlined by [11]–[14]. This algorithm demonstrates the utility of our mechanism and we acknowledge that alternative control approaches may achieve superior results.

We control quadrotor position in the horizontal plane using nested PD/PID control loops. The inner PD loop takes as input desired roll, pitch, and yaw angles, and outputs torques. The outer PID loop takes as input a desired position in x and y and outputs roll and pitch angles. We use a separate PD control law to achieve desired z position. We employ this strategy in order to set virtual desired heights above and below the docking mechanism as a way of instructing an increase or decrease in thrust for interfacing with the mechanism. We generate a trajectory for the quadrotor to follow for moving to a new desired position.

Figure 6 explains our algorithm for a quadrotor to relocate the mechanism. There are four main blocks: 1) the quadrotor docks to the mechanism; 2) the quadrotor detaches the connected mechanism from the metal surface; 3) the quadrotor attaches the connected mechanism to a new location; 4) the quadrotor undocks from the mechanism. We begin by setting a desired grasp location, S^*, and a desired placement location, G^*, and proceeding towards S^* for docking.

1) Docking begins by the quadrotor aligning itself underneath the mechanism within a cylindrical volume that extends from the housing funnel of the mechanism. The boundaries of this volume are defined by an upper and lower proximity to the mechanism and a cylindrical radius ϵ. The ϵ-region is shown in Figure 7. Once aligned, the desired z position, Z^*, is moved on a trajectory with velocity κ towards a virtual position above the mechanism. The controller moves the quadrotor along this trajectory, sending the insertion component mounted to the quadrotor towards the housing component of the mechanism. If the parts successfully connect, docking is complete. Two failure cases are diagnosed and remedied: (i) the quadrotor leaves the γ-region or (ii) the quadrotor thrusts upward for some time but components fail to mate. Failure results in realignment and another docking attempt.
2) Detaching begins by moving Z^* to a virtual position below the quadrotor. The controller decreases thrust to allow the quadrotor to fall to Z^*. With enough of a thrust decrease, the gravitational force outweighs the pull force of the magnet and the mechanism releases from the attached surface.
3) Attaching is done by moving towards G^* and repeating the docking process. If the magnets hold to the surface, attaching is complete. Failure will occur if the quadrotor misses G^* or the magnets fail to hold. Failure results in realignment and another attaching attempt.
4) Undocking begins by setting Z^* to a virtual position above the mechanism, prompting the controller to

	κ (m/s)	ϵ	P	T_s	T_f	$\mathbb{E}[T_D]$
1	-0.50	γ	0.33	7.02	3.39	13.80
2	-0.50	$\gamma/2$	0.19	7.02	3.64	22.77
3	-0.50	$\gamma/4$	0.28	7.02	3.61	16.40
4	-0.50	$\gamma/8$	0.35	7.01	6.69	19.27
5	-0.33	γ	0.18	9.51	3.43	24.71
6	-0.33	$\gamma/2$	0.14	9.52	4.13	35.36
7	-0.33	$\gamma/4$	0.36	9.52	3.17	15.23
8	-0.33	$\gamma/8$	0.37	9.52	6.95	21.32
9	-0.25	γ	0.29	12.02	2.41	18.04
10	-0.25	$\gamma/2$	0.24	12.02	5.09	28.00
11	-0.25	$\gamma/4$	0.36	12.01	2.88	17.05
12	-0.25	$\gamma/8$	0.30	12.01	9.21	33.51
13	-0.20	γ	0.28	14.51	3.39	23.33
14	-0.20	$\gamma/2$	0.14	14.51	5.51	47.55
15	-0.20	$\gamma/4$	0.29	14.52	5.27	27.16
16	-0.20	$\gamma/8$	0.16	14.51	9.68	65.32

TABLE I: Expected docking times ($\mathbb{E}[T_D]$).

thrust upward. After an allotted amount of time, Z^* is moved to a new position below the quadrotor. The controller decreases thrust for the quadrotor to fall to the new Z^*. If the quadrotor falls to the new Z^*, undocking is complete and a new S^* and G^* can be set. However, failure occurs if the quadrotor is unable to break free and reach Z^*. The undocking procedure is repeated until success.

IV. EXPERIMENTAL RESULTS

For our experiments, we use a commercially available Ascending Technologies Hummingbird quadrotor [15]. Quadrotor pose estimates are captured with a motion capture system and position control is transmitted from a ground station to the quadrotor using wireless XBee modules.

A. Picking κ and ϵ

We run docking experiments to determine values for κ and ϵ that achieve the minimum expected docking time. We use a Markov chain model (Figure 8) where we begin in a ready state and attempt to dock with a success probability of P that takes time T_s and a failure probability of $Q = (1 - P)$ that takes time T_f. We estimate P, T_s, and T_f empirically. We then calculate the expected docking time ($\mathbb{E}[T_D]$) which can be written as an infinite series

$$\begin{aligned}\mathbb{E}[T_D] =& PT_s + PQ(T_s + T_f) + PQ^2(T_s + 2T_f) + ... \\ =& (PT_s \sum_{i=0}^{\infty} Q^i) + (PT_f \sum_{i=0}^{\infty} iQ^i) \\ =& (\mathbb{S}_1) + (\mathbb{S}_2).\end{aligned} \tag{6}$$

Note that $\mathbb{S}_1$ is a geometric series. By defining $a_1 = PT_s$ and $r_1 = Q$, we can write

$$\mathbb{S}_1 = \frac{a_1}{1 - r_1} = \frac{PT_s}{1 - (1 - P)} = T_s. \tag{7}$$

Similarly, $\mathbb{S}_2$ is a polylogarithm ($Li_s(z_2)$) where $s = -1$. By Defining $a_2 = PT_f$, and $z_2 = Q$, we can write

$$\mathbb{S}_2 = a_2 Li_s(z_2) = \frac{a_2 z_2}{(1 - z_2)^2} = \frac{T_f(1 - P)}{P}. \tag{8}$$

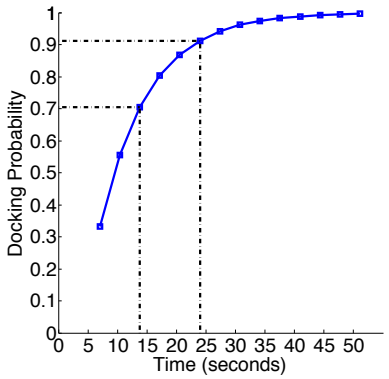

Fig. 9: Docking probability vs. time with $\kappa = -0.5\ m/s$ and $\epsilon = \gamma$.

Thus, the expected docking time can be written as

$$\mathbb{E}[T_D] = T_s + \frac{T_f(1 - P)}{P}. \tag{9}$$

We choose four κ $(-0.50, -0.33, -0.25, -0.20)$ and ϵ $(\gamma = 0.0425m, \gamma/2, \gamma/4, \gamma/8)$ values to test, resulting in 16 permutations. For safety reasons, we bound κ at $-0.50\ m/s$. We run 320 trials (20 trials per permutation) and document success/failure and the time for success(T_s)/recovery(T_f) respectively. Table I shows the empirical probability of success (P), mean time for success (T_s) and failure (T_f), and expected docking time ($\mathbb{E}[T_D]$).

From Table I, the parameters with the minimum expected docking time of $\mathbb{E}[T_D] = 13.80$ are $\kappa = -0.50\ m/s$ and $\epsilon = \gamma$. This permutation of parameters corresponds to $P = 0.33$, which is not the highest empirical success probability. In fact, parameter values for permutation numbers 3, 4, 7, 9, and 11 all correspond to smaller expected docking times than the expected docking time of permutation 8 (the highest empirical success probability). This result shows that if our design goal is to minimize the flight time, the success probability is not indicative of the optimal parameter values.

In Figure 9, we plot the probability of docking vs. time given our chosen parameters: $\kappa = -0.50\ m/s$ and $\epsilon = \gamma$. There is more than a 70% chance of successfully docking after 13.80 seconds (inner dashed black line) and more than a 90% chance of successfully docking after 25 seconds.

B. Determining Mechanism Success and Failure

Figure 11 displays two time-aligned plots (one above the other) of docking followed by undocking. For illustrative purposes, we selected a rare case where several different failure types occur prior to success. The top plot shows (i) the distance of the center of mass of the quadrotor from that of the docking mechanism in the xy-plane (solid blue line) and (ii) the threshold that, when crossed, aborts the attempt as a failure (dashed green line). The bottom plot shows (i) the actual z position of the quadrotor (solid blue line), (ii) the desired z position of the quadrotor (dashed green line), and (iii) the locations and types of failures (solid red lines).

In Figure 11, the first failure is diagnosed between 22 and 23 seconds. Prior to the failure, the decreasing desired z

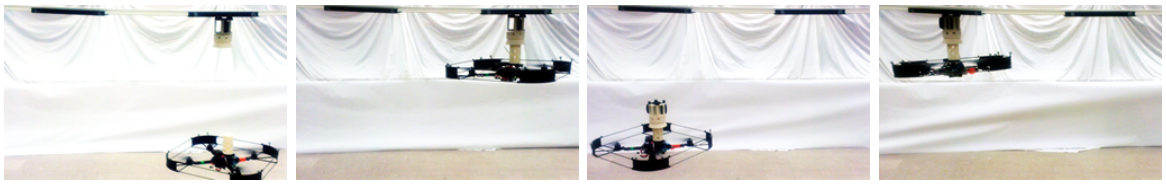

(a) (b) (c) (d)

Fig. 10: Snapshots of wireless camera relocation demo.

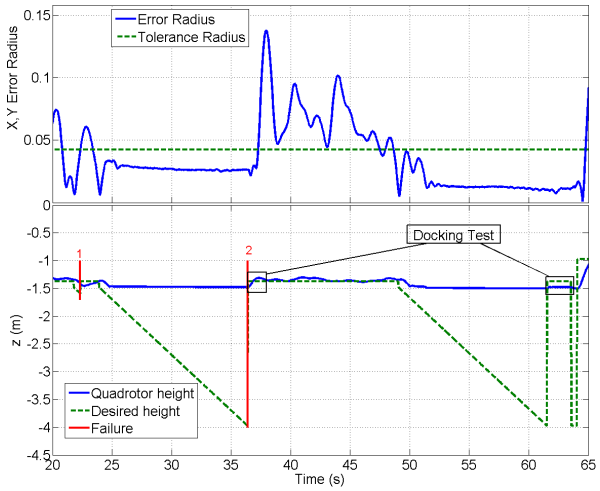

Fig. 11: Diagnosing failures and determing docking success.

indicates a docking attempt. The xy-distance within this same time frame is low at first, then moves above the threshold. This is a failure due to the center of mass of the quadrotor leaving the γ-region defined in Figure 7.

The second failure occurs between 36 and 37 seconds. Prior to the failure, the desired z decreases, indicating a docking attempt. In this case, the xy-distance is within the threshold. Therefore, the failure is caused by the pieces failing to connect. To detect this failure, we compare to the successful docking that takes place between 62 and 63 seconds. Both of these zones are labeled as docking tests. When docking is a success, the actual z is unable to reach the desired z because the quadrotor is fixed to the mechanism. When docking fails, the actual z reaches the desired z.

After successful docking, the quadrotor attempts to undock. This is identifiable in the plot because the actual z position is able to reach the desired z position. In the event of a failed undocking attempt, the actual z position does not change because the quadrotor is still fixed to the mechanism.

C. Relocating Cameras

Figure 10 shows snapshots of a quadrotor successfully using our mechanism to relocate cameras on the underside of a steel surface. We define three zones (A, B, C) to represent unique locations on a steel beam and a fourth zone (D) as the waypoint. The quadrotor is then commanded to grab the mechanism and move it to the next location. After each placement, the UAV returns to zone D before proceeding to the next zone. We use this demonstration as a proof of concept for relocating cameras on a construction site and leave a motion capture free control strategy for future work.

V. CONCLUSION

In this paper, we presented a passive mechanism that enables a quadrotor to relocate objects. We focused on the design of the mechanism and a proof-of-concept demonstration of camera relocation on a construction site. In the future, we plan to extend this work by implementing monocular camera based control for docking, relocation, and undocking.

ACKNOWLEDGMENT

This work was supported by the National Science Foundation (CMMI-1446765) and the Department of Defense through the NDSEG Fellowship program.

REFERENCES

[1] C. Doyle, J. Bird, T. Isom, J. Kallman, D. Bareiss, D. Dunlop, R. King, J. Abbott, and M. Minor, "An avian-inspired passive mechanism for quadrotor perching," *IEEE/ASME Trans. Mech.*, 2013.

[2] D. Mellinger, Q. Lindsey, M. Shomin, and V. Kumar, "Design, modeling, estimation and control for aerial grasping and manipulation," in *IEEE/RSJ IROS*, 2011.

[3] J. Thomas, J. Polin, K. Sreenath, and V. Kumar, "Avian-Inspired Grasping for Quadrotor Micro UAVs," in *ASME IDETC/CIE*, 2013.

[4] S. B. Backus, L. U. Odhner, and A. M. Dollar, "Design of hands for aerial manipulation: Actuator number and routing for grasping and perching," in *IEEE/RSJ IROS*, 2014.

[5] T. Danko and P. Oh, "Design and control of a hyper-redundant manipulator for mobile manipulating unmanned aerial vehicles," *J. Intel and Robot. Sys.*, 2014.

[6] A. Q. L. Keemink, M. Fumagalli, S. Stramigioli, and R. Carloni, "Mechanical design of a manipulation system for unmanned aerial vehicles," in *IEEE ICRA*, 2012.

[7] M. Fumagalli, R. Naldi, A. Macchelli, F. Forte, A. Keemink, S. Stramigioli, R. Carloni, and L. Marconi, "Developing an aerial manipulator prototype: Physical interaction with the environment," *IEEE Robot. Auto. Mag.*, 2014.

[8] M. Golparvar-Fard and Y. Ham, "Automated diagnostics and visualization of potential energy performance problems in existing buildings using epar-energy performance augmented reality-models," *JCCEE*, 2012.

[9] L. A, "Propel and repel ball point pen mechanism," 1972, uS Patent 3,679,318. [Online]. Available: http://www.google.com/patents/US3679318

[10] J. Handley, "Cam follower mechanism," 1966, uS Patent 3,263,512. [Online]. Available: http://www.google.com/patents/US3263512

[11] S. Bouabdallah, P. Murrieri, and R. Siegwart, "Design and control of an indoor micro quadrotor," in *IEEE ICRA*, 2004.

[12] S. Bouabdallah and R. Siegwart, "Full control of a quadrotor," in *IEEE/RSJ IROS*, 2007.

[13] P. Corke, *Robotics, Vision and Control - Fundamental Algorithms in MATLAB®*, 2011.

[14] R. Mahony, V. Kumar, and P. Corke, "Multirotor aerial vehicles: Modeling, estimation, and control of quadrotor," *IEEE Robot. Auto. Mag.*, 2012.

[15] Ascending Technologies, GmbH, http://www.asctec.de.